Red blood cell partitioning and blood flux redistribution in microvascular bifurcation

Yuanqing Xu,[1] Fangbao Tian,[2, a)] Hanjun Li,[1] and Yulin Deng[1]
[1)] *School of Life Science, Beijing Institute of Technology, Beijing 100081, China*
[2)] *Department of Mechanical Engineering, Vanderbilt University, 2301 Vanderbilt Place, Nashville, Tennessee 37235-1592, USA*

(Received 3 December 2011; accepted 10 January 2012; published online 10 March 2012)

Abstract This paper studies red blood cell (RBC) partitioning and blood flux redistribution in microvascular bifurcation by immersed boundary and lattice Boltzmann method. The effects of the initial position of RBC at low Reynolds number regime on the RBC deformation, RBC partitioning, blood flux redistribution and pressure distribution are discussed in detail. It is shown that the blood flux in the daughter branches and the initial position of RBC are important for RBC partitioning. RBC tends to enter the higher-flux-rate branch if the initial position of RBC is near the center of the mother vessel. The RBC may enter the lower-flux-rate branch if it is located near the wall of mother vessel on the lower-flux-rate branch side. Moreover, the blood flux is redistributed when an RBC presents in the daughter branch. Such redistribution is caused by the pressure distribution and reduces the superiority of RBC entering the same branch. The results obtained in the present work may provide a physical insight into the understanding of RBC partitioning and blood flux redistribution in microvascular bifurcation. [doi:10.1063/2.1202401]

Keywords immersed boundary, lattice Boltzmann method, red blood cell, microvascular bifurcation

Red blood cell (RBC) partitioning and blood flux redistribution in microvascular bifurcation are very important in the microvasculature.[1] For example, the performance of the microvascular bifurcation affects the microvascular oxygen distribution, the effective viscosity of blood in microvessels, and the distribution of other metabolites.[2–4] Therefore, a more thorough understanding of RBC partitioning and blood flux redistribution in microvascular bifurcation is desirable to aid understanding and quantification of microvascular transport in normal and disease states.

Extensive experiments[1,2] and numerical simulations[4–8] have studied the RBC motion in microvascular bifurcation. For the capillary bifurcations of diameters ranging from 5 to 15 μm, the upstream hematocrit distribution at a small diverging bifurcation plays a significant role on RBC partitioning.[1] In the arteriolar bifurcations of diameters in the range of 10–30 μm, the higher-flow-rate branch generally receives a higher hematocrit if the downstream branches are similar in size.[2] In addition, the RBC preferentially enters the higher-flux-rate branch, leading to unequal discharge hematocrit in the downstream branches. For unequally-sized daughter vessels, partitioning is asymmetric, with RBCs tending to enter the smaller vessel.[4] Though the Reynolds number of the RBC moving in microvascular bifurcation is much less than one, the RBC model can drift across background fluid streamlines.[5,6] Studies found that if two closed RBCs going through bifurcation, the first RBC tends to enter the high-flow-rate branch, while the second tends to enter the other.[7,8] Recently, the behaviors of RBC and liposome-encapsulated hemoglobin in microvascular bifurcation were studied.[9] It is found that the partial replacement of RBC by liposome-encapsulated hemoglobin reduces the bias of oxygen flux and liposome-encapsulated hemoglobin reduces contribution in reducing the heterogeneity of oxygen supply. Though significant progresses have been made in understanding of RBC behavior in microvascular bifurcation, RBC partitioning and blood flux redistribution in microvascular bifurcation are still not clear and need to be further studied.

In the present work, an improved immersed boundary method based on lattice Boltzmann method is employed to study RBC partitioning and blood flux redistribution in microvascular bifurcation. The deformation of RBC, the flow rate in the microvascular bifurcation and the pressure distribution are studied in detail.

As shown in Fig. 1, we consider a microvessel with bifurcation, which is symmetrical and composed of one 10 μm-diameter mother vessel and two 5 μm-diameter daughter branches. A cylinder is taken as the initial configuration of the RBC. The blood plasma and the RBC cytoplasm are governed by the incompressible Navier-Stokes equations

$$\rho\left(\frac{\partial \boldsymbol{u}}{\partial t} + \boldsymbol{u}\cdot\nabla\boldsymbol{u}\right) = \nabla\cdot\boldsymbol{T} + \boldsymbol{f}, \tag{1}$$

$$\nabla\cdot\boldsymbol{u} = 0, \tag{2}$$

where ρ is the density of the fluid, $\boldsymbol{u}$ is the velocity, p represents the pressure, $\boldsymbol{f}$ denotes the body force, $T_{ij} = -p\delta_{ij} + \mu(\partial u_i/\partial x_j + \partial u_j/\partial x_i)$ is the stress with μ being the viscosity of the fluid. For both blood plasma and the RBC cytoplasm, the density is $\rho = 1.00$ g/cm^3.

[a)] Corresponding author. Email: fangbao.tian@vanderbilt.edu.

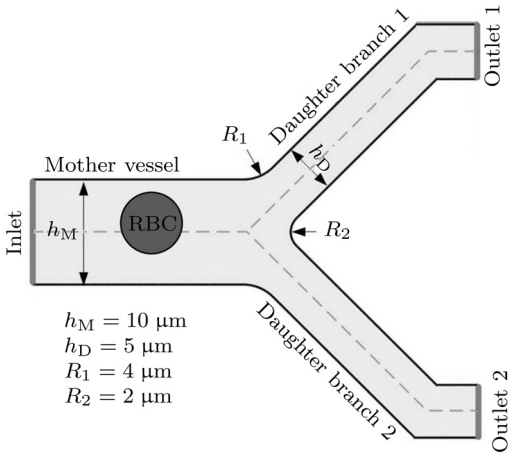

Fig. 1. The sketch of the RBC in microvascular bifurcation.

The viscosities of the plasma and the RBC cytoplasm are $\mu_p = 1.2$ cp and $\mu_c = 6$ cp, respectively.

The motion of the RBC is described by[10–13]

$$\boldsymbol{F}(s,t) = \boldsymbol{F}_s(s,t) - \boldsymbol{F}_b(s,t), \tag{3}$$

where s is the arc length along the membrane, $\boldsymbol{F}_s(s,t)$ is the membrane extensional force caused by stretching or compressing in the tangent direction and calculated by $\boldsymbol{F}_s(s,t) = (\partial/\partial s)\left[\boldsymbol{T}(s)\partial \boldsymbol{X}(s,t)/\partial s\right]$ with $\boldsymbol{T}(s) = K_s(|\partial \boldsymbol{X}(s,t)/\partial s| - 1)$ and K_s the extensional rigidity. The $\boldsymbol{F}_b(s,t)$ is the membrane bending force. Using Euler-Bernoulli beam theory, we can describe the bending force as $\boldsymbol{F}_b(s,t) = (\partial^2/\partial s^2)\left[K_b \partial^2 \boldsymbol{X}(s,t)/\partial s^2\right]$. The $\boldsymbol{F}$ is the fluid force on the RBC. The initial diameter of the RBC is 6 μm. The non-dimensional stretching coefficient K_s and bending rigidity K_b are 0.6 and 0.2, respectively.

In this study, the microvessel wall is rigid and the velocity on the wall is zero. On the RBC membrane, the velocity of the fluid equals that of the membrane. The flow is driven by the pressure and thus, the pressure on the inlet and outlets are prescribed. To produce asymmetrical blood flow rate in the downstream branches, the pressures on the two outlets are slightly different. The typical parameters described above are chosen based on experimental visualizations and previously numerical simulations of typical RBC motion in microvascular bifurcation.[1,2,4,7,8,14–17]

The fluid-structure interaction is solved at low Reynolds numbers using an improved immersed boundary method coupled with a lattice Boltzmann method. In the simulation, the computational domain is divided into square grid of 215 lattices in the horizontal direction and 197 lattices in the vertical direction. The lattice size is $\mathrm{d}x = \mathrm{d}y = 1$, which represents a physical length of 0.2 μm. The pressures are 2 Pa, 0.6 Pa and 0 Pa on the inlet, outlet 1 and outlet 2, respectively.

In this study, we will focus on RBC partitioning and blood flux redistribution by changing the initial vertical position of the RBC. To do this, we define the vertical coordinate difference between the central line of the mother vessel and the center of the RBC as $\mathrm{d}y_i = y_i - y_0$, where y_0 and y_i are the vertical coordinates of the central line of the mother vessel and the center of the RBC, respectively. In the present study, $\mathrm{d}y_i = 0$ μm, 0.8 μm and 1.6 μm.

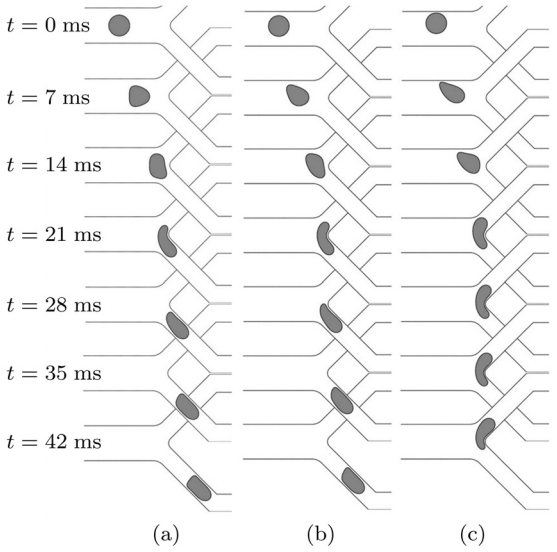

Fig. 2. RBC deformation and partitioning in microvessel bifurcation: (a) $\mathrm{d}y_i = 0$μm, (b) $\mathrm{d}y_i = 0.8$ μm, and (c) $\mathrm{d}y_i = 1.6$ μm.

We first discuss RBC deformation and partitioning. The instantaneous snapshots of the RBC configuration are shown in Fig. 2. When the RBC is initially located near the central line, as $\mathrm{d}y_i = 0$ μm, the configuration of the RBC in the mother vessel upstream of the bifurcation point is similar to bullet shape (see $t = 7$ ms in Fig. 2(a)). When the surface of the RBC is close to the vessel boundary, the shear flow makes the RBC tear-shaped, as shown in Figs. 2(b) and 2(c). The RBC of $\mathrm{d}y_i = 0$ μm and 0.8 μm tends to enter the branch of lower outlet pressure, which is revealed by Figs. 2(a) and 2(b) and consistent with the previous studies.[2,4] But if the RBC is close to the up wall of mother vessel, as $\mathrm{d}y_i = 1.6$ μm, it will enter daughter branch 1, of which the outlet pressure is higher. Therefore, the initial position could affect RBC deformation and partitioning. If an RBC is randomly located in the mother vessel, it has more opportunity to enter the branch of lower outlet pressure.

As discussed in the previous section, the initial position of RBC and the blood flux in the daughter branches are very important in determining RBC partitioning. To demonstrate the effect of the blood flux, here we discuss the relationship of the motion of RBC and blood flux redistribution at $\mathrm{d}y_i = 0.8$ μm.

The velocity profiles on the inlet, outlet 1 and outlet 2 at three typical instants are shown in Fig. 3 which

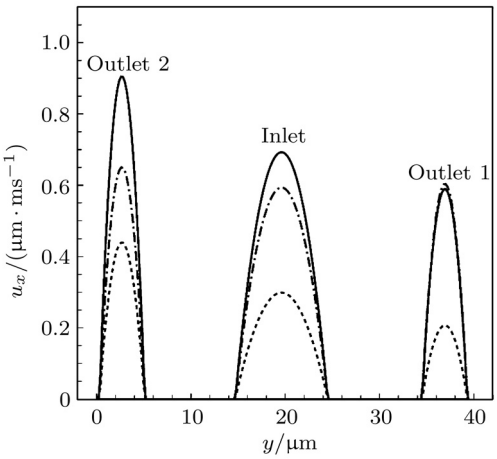

Fig. 3. Velocity profiles on the inlet, outlet 1 and outlet 2 at three typical instants: $t = 0$ ms (solid line), $t = 21$ ms (dashed line) and $t = 42$ ms (dash-dotted line).

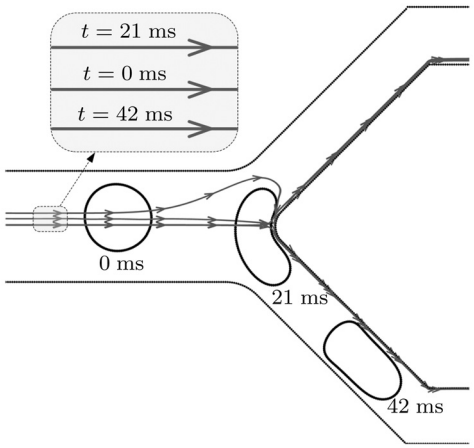

Fig. 4. Streamlines passing the bifurcation point and configurations of RBC at three typical instants.

has several interesting implications. First, the blood flux of daughter branch 2 is initially higher than daughter branch 1. The higher blood flux causes the fact that RBC tends to enter daughter branch 2. Second, when RBC gets close to the bifurcation point, as $t = 21$ ms, the totally blood flux is depressed by the block effect of RBC (also refer to Fig. 4 showing the streamlines passing through the stagnation point and RBC configurations at three typical instants). Last, the blood flux of daughter branch 1 recovers when RBC enters daughter branch 2, as shown in Fig. 4 at $t = 42$ ms. But the flux of daughter branch 2 is still less than that without RBC. It is noted from Fig. 4 that RBC drifts across the background streamlines when moving downward in the mother vessel, which is consistent with the previous studies.[5,6] The drift makes RBC below the streamline pass the bifurcation point when it is near the bifurcation point. If the initial position of RBC is very close to the top wall of the mother vessel, as $\mathrm{d}y_i = 1.6$ μm, RBC can not drift to the bottom side of the streamline passing the bifurcation point, and thus it will enter daughter branch 1.

Pressure is an important quantity in blood circulation system for determining the blood balance and driving the motion of RBC. In vivo experiment, it is a challenge to measure the pressure distribution in the microvessel, while in the numerical experiment, it is convenient to present the pressure distribution. As a typical case, the pressure distribution of $\mathrm{d}y_i = 0.8$ μm at three instants are shown in Fig. 5. At $t = 0$ ms, RBC does not have significant effect on the pressure distribution due to the facts that the density of RBC is the same as ambient blood and the shear flow rate near RBC is weak. It is noted from Figs. 5(a) and 5(b) that the gradient of pressure in daughter branch 2 is larger than daughter branch 1 and thus the blood flux in daughter branch 2 is higher, which straightforwardly considers the fluid dynamical theory.[18] When RBC reaches the bifurcation point (as shown in Fig. 5(c) at $t = 21$ ms), the deformation of RBC is dramatic and the pressure in RBC is higher than that of the ambient fluid, which is further demonstrated by Fig. 5(d). This type of local elevation of pressure is a threat to human health.[19] When RBC enters the daughter branch 2, as shown in Fig. 5(e) at $t = 42$ ms, there are several interesting observations in the pressure distribution. First, the pressure gradients at two daughter branches are almost the same at the upstream of RBC, leading to the approximately equal blood flux in both daughter branches, as shown in Fig. 3. Second, the pressure jump across RBC still exists but its intensity decreases. Last, the pressure gradient increases in daughter branch 2 downstream of RBC by the presence of RBC compared to $t = 0$ ms (see Figs. 5(b) and 5(f)).

The RBC partitioning and blood flux redistribution in microvascular bifurcation are studied by immersed boundary–lattice Boltzmann method. The RBC deformation, RBC partitioning, blood flux redistribution and pressure distribution are discussed in detail by varying the initial position of RBC. Our simulations show that the blood flux in the daughter branches and the initial position of RBC are important for RBC partitioning. Specifically, RBC tends to enter the higher-flux-rate branch, which is also the branch of lower outlet-pressure. In addition, the blood flux is redistributed when an RBC presents in the daughter branch. Such redistribution is caused by the pressure distribution and reduces the superiority of RBC entering the same branch.

In the future work, the three-dimensional effect, multiple RBCs and interaction between RBCs will be considered. Furthermore, the oxygen and other substance dissolved in the blood also can be incorporated.

This work was supported by Excellent Young Teachers Program (3160012261-001) and Fund for Basic Research (3160012211104) of Beijing Institute of Technology, and partly supported by the National Key Technology R&D Program (2009BAK59B01).

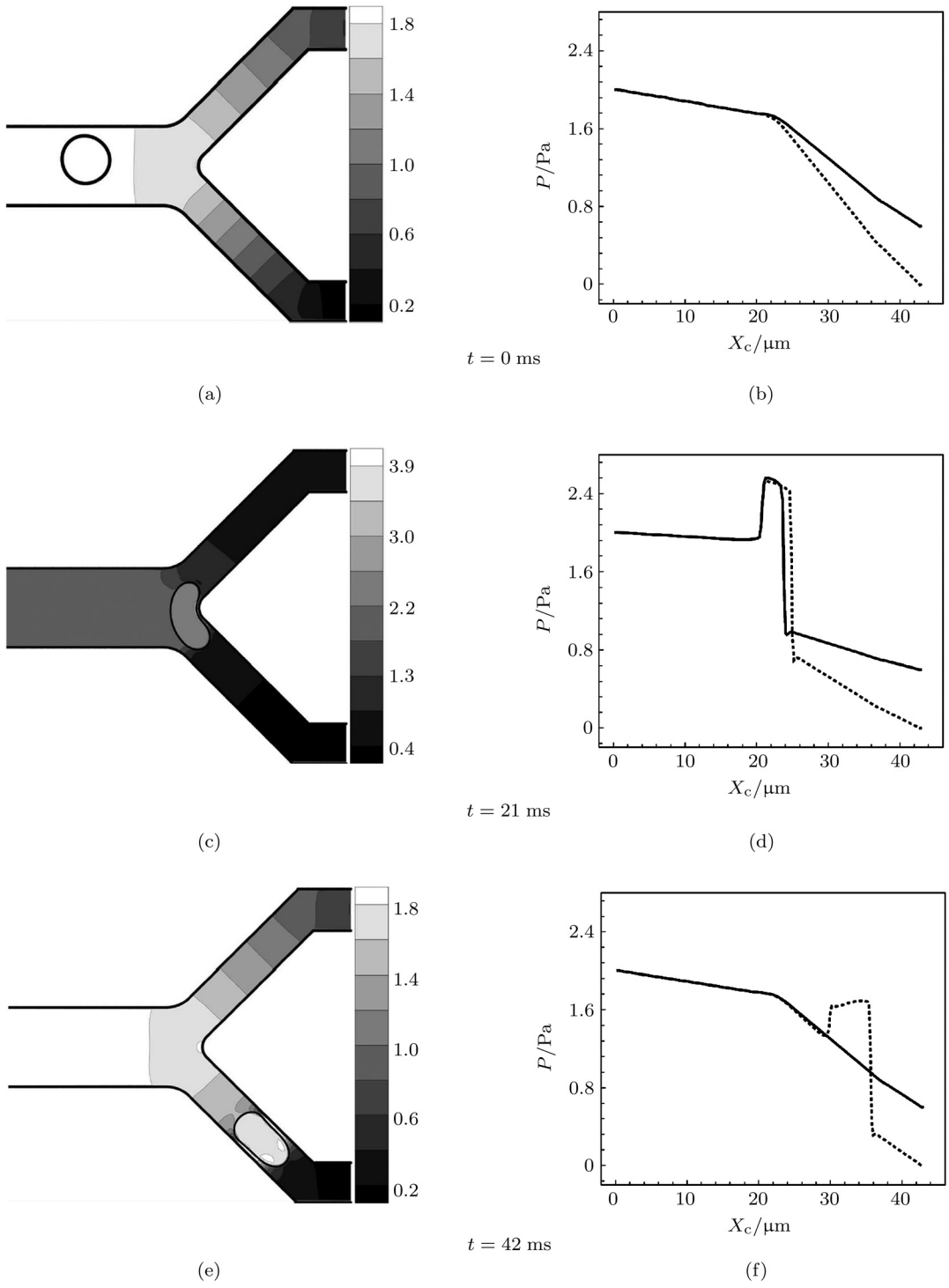

Fig. 5. Pressure distribution at three instants: (a), (c) and (e) are the pressure field in the vessel; (b), (d) and (f) are the pressure distributions along the centerline of the vessel. In (b), (d) and (f), the solid line is the mother vessel–daughter branch 1, the dashed line is the mother vessel–daughter branch 2, and x_c is the horizontal coordinate along the centerline.

1. G. W. Schmid-Schonbein, R. Skalak, and S. Usami, et al, Microvasc. Res. **19**, 18 (1980).
2. A. R. Pries, K. Ley, amd M. Claassen, et al, Microvasc. Res. **38**, 81 (1989).
3. A. R. Pries, T. W. Secomb, and P. Gaehtgens, Cardiovasc. Res. **32**, 654 (1996).
4. J. O. Barber, J. P. Alberding, and J. M. Restrepo, et al, Annals Biomed. Eng. **36**, 1690 (2008).
5. D. M. Audet, and W. L. Olbricht, Microvasc. Res. **33**, 377 (1987).

6. A. W. El-Kareh, and T. W. Secomb, Int. J. Mult. Flow **26**, 1545 (2000).
7. C. Pozrikidis, *Computational Hydrodynamics of Capsules and Biological Cells* (Taylor and Francis Group/CRC Press, Cambridge, 2010).
8. T. W. Secomb, J. O. Barber, and J. P. Alberding, et al, In: XXII ICTAM Conference, Adelaide, Australia, 1390–1395 2008.
9. T. Hyakutake, S. Tominaga, and T. Matsumoto, et al, J. Biomech. Eng. **130**, 011014 (2008).
10. L. Zhu, and C. S. Peskin, J. Comput. Phys. **179**, 452 (2002).
11. F. B. Tian, H. Luo, and L. Zhu, et al, Phys. Rev. E **82**, 026301 (2010).
12. F. B. Tian, H. Luo, and L. Zhu, et al, J. Comput. Phys. **230**, 7266 (2011).
13. F. B. Tian, H. Luo, and L. Zhu, et al, Phys. Fluids, **23**, 111903 (2011).
14. R. T. Carr, and L. L. Wickham, Microvasc. Res. **40**, 179 (1990).
15. M. Lagoela, B. Oliveira, and D. Cidre, et al, In: Computational Vision and Medical Image Processing: Vip-IMAGE 2009, edited by J. M. R. S. Tavares (2009).
16. J. O. Barber, J. M. Restrepo, and T. W. Secomb, Cardiovasc. Eng. Tech. **1** (2011). 10
17. W. Xiong, and J. Zhang, Biomech. Mod. Mechanobio. DOI: 10.1007/s10237 (2011).
18. G. K. Batchelor, *An Introduction to Fluid Dynamics* (Cambridge University Press, Cambridge, 1967).
19. C. H. Heldin, K. Rubin, and K. Pietras, et al, Nature Rev. Cancer **4**, 806 (2004).